Role of Heme Distortion on Oxygen Affinity in Heme Proteins: The Protoglobin Case

Damián E. Bikiel,[†] Flavio Forti,[‡] Leonardo Boechi,[†] Marco Nardini,[§] F. Javier Luque,[‡] Marcelo A. Martí,[†,||,*] and Darío A. Estrin[†,*]

Departamento de Química Inorgánica, Analítica y Química Física/INQUIMAE-CONICET, Facultad de Ciencias Exactas y Naturales, Universidad de Buenos Aires, Ciudad Universitaria, Pabellón 2, Buenos Aires, C1428EHA, Argentina, Departament de Fisicoquímica and Institut de Biomedicina (IBUB), Facultat de Farmàcia, Universitat de Barcelona, Av. Diagonal 643, 08028, Barcelona, Spain, Department of Biomolecular Sciences and Biotechnology, CNR-INFM, University of Milano, Milano, Italy, and Departamento de Química Biológica, Facultad de Ciencias Exactas y Naturales, Universidad de Buenos Aires, Ciudad Universitaria, Pabellón 2, Buenos Aires, C1428EHA, Argentina

Received: March 9, 2010

The chemical properties of heme proteins largely reflect the electronic properties of their heme group. Often, the porphyrin ring of the heme exhibits significant distortions from its isolated structure, but the impact of these distortions on the chemical properties of the heme is yet uncertain. A systematic study focused on the effects of the distortion of the macrocycle on the binding affinity for oxygen is presented. The results show that out-of-plane distortions decrease the binding affinity, while in-plane distortions can increase or decrease it. Among in-plane distortions, only the *breathing* mode, which involves the symmetric compression−expansion of the porphyrin ring, strongly modulates the binding affinity. These findings shed light into the peculiar binding affinity of *Methanosarcina acetivorans* protoglobin, a protein that contains a highly distorted heme. Overall, the results highlight that in-plane distortions might be exploited by certain classes of heme proteins to modulate the ligand affinity.

Introduction

Heme proteins can play a wide variety of functional roles including storage and transport of small ligands, redox processes, or sensing of diatomic compounds. Valuable qualitative indications about the role of heme proteins come from the binding properties of small diatomic ligands, such as the kinetic rate constants of ligand association (k_{on}) and dissociation (k_{off}) processes.[1,2] Typical k_{on} values range from 10^5 to 10^8 M^{-1} s^{-1}, while k_{off} values can vary by up to 7 orders of magnitude (from 10^{-3} to 10^4 s^{-1}).[3,4] O_2 storage or transport proteins (such as myoglobin, Mb, or hemoglobin, Hb) display moderate affinities ($K_{O_2} \approx 1$ μM^{-1}) with large association rates and moderate to high dissociation rate constants ($1-10$ s^{-1}). In contrast, proteins acting as NO dioxygenases, such as *Ascaris* Hb (AscHb)[5] or *M. tuberculosis* truncated Hb N (*Mf*TrHbN), display high O_2 affinities due to low or very low dissociation rate constants ($0.001-0.1$ s^{-1}).[6] Clearly, understanding the factors that modulate ligand affinity is crucial for a comprehensive knowledge of the physiological role of heme proteins and has been a constant effort of many different research groups over the past few decades.[7]

Association processes mainly depend on the accessibility of ligands to the heme distal site, which can involve either a gated mechanism, as in Mb,[8] or even migration through cavities/tunnels, as in truncated Hbs.[9,10] Dissociation rate constants are determined by various factors such as the interaction between the ligand and the heme (i.e., the strength of the Fe-ligand bond), the interactions between the ligand and the surrounding protein matrix (i.e, hydrogen-bond (HB) or other forms of noncovalent interactions with distal residues that can either be stabilizing or destabilizing) and the probability of escape from the ligand pocket. For instance, the very low O_2 dissociation from oxygenated *Mf*TrHbN can be attributed to multiple HB interactions with TyrB10 and GlnE11 residues.[6,11] In other cases, like leghemoglobin, the strength of the Fe−O bond can be further modulated by proximal interactions.[12] Ligand escape has also been found to be a key issue in determining kinetic constants, specifically k_{off}.[13]

Collman[14] and Ibers[15] studied synthetic models of porphyrins to shed light into the steric effect of the environment on the binding of CO and O_2 in heme proteins, principally by strains over the ligand. However, a much less studied factor in controlling the intrinsic heme reactivity concerns the distortions of the porphyrin ring due to the protein environment. The reason for such a lack of investigation on porphyrin distortion and heme reactivity may be related to the limited experimental resolution achieved in many crystallographic investigations that did not allow mapping with the required precision the contained deviations from planarity of the porphyrin system. A systematic classification of heme distortions, referred to as normal-coordinate structural decomposition (NSD), has been proposed by Jentzen et al.,[16] who identified the most relevant out-of-plane (saddling, ruffling, doming, X-waving, Y-waving, and propellering) and in-plane (meso-stretching, N-pyrrole stretching, pyrrole traslation (X,Y), breathing, and pyrrole rotation) normal modes that relate the structure of a distorted heme compared to a reference D_{4h} structure (see Figure 1).[17,18] Noteworthy, it has been shown that different heme protein families retain similar heme distortions.[16]

A highly distorted heme has recently been found in *Methanosarcina acetivorans* protoglobin (Pgb),[19] which is a single domain archeal heme protein related to the globin domain of

* To whom correspondence should be sent. E-mail: D.A.E., dario@qi.fcen.uba.ar; M.A.M., marcelo@qi.fcen.uba.ar.
[†] Departamento de Química Inorgánica, Universidad de Buenos Aires.
[‡] Universitat de Barcelona.
[§] University of Milano.
[||] Departamento de Química Biológica, Universidad de Buenos Aires.

10.1021/jp102135p
Published on Web 06/04/2010

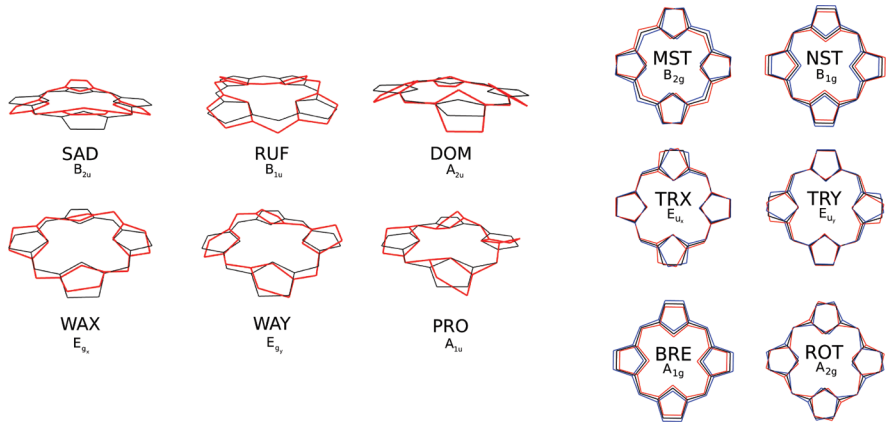

Figure 1. Heme distortions. Left: out-of-plane distortions (red) are doming (*dom*), ruffling (*ruf*), saddling (*sad*), waving (*wax*, *way*) and propellering (*pro*). Right: positive (red) and negative (blue) in-plane distortions involving meso-stretching (*mst*), *N*-pyrrole stretching (*nst*), pyrrole traslation (*trx*, *try*), breathing (*bre*), and pyrrole rotation (*rot*). The reference D_{4h} structure is shown in black.

globin-coupled sensor proteins.[20−22] Pgb can bind O_2 reversibly in vitro, but the very low O_2 dissociation rate (0.092−0.0094 s^{-1}) is completely unexpected as there is no distal HB stabilization of the heme-bound O_2.[19] In addition, inspection both of X-ray structure and of the molecular dynamics trajectory show an accessible heme moiety, suggesting that no ligand escape effect is present. This structural feature raises challenging questions about the precise function of Pgb, and particularly on the effect of the unusual heme distortion on Pgb reactivity.[21,22]

Heme distortions have been suggested to modulate heme reactivity in proteins. Thus, the effect of the out-of-plane distortions on properties such as the UV−vis spectrum, redox potential, and ligand affinity has been examined in recent studies.[23−30] Moreover, the significant ruffling observed in nitrophorins has been related to the relative stability of the ferrous/ferric states.[23] Finally, heme distortions in nitric oxide synthase have been related to a subtle tuning of its electronic structure.[31] Nevertheless, to the best of our knowledge, there is no systematic study of the effect of heme distortions on ligand binding affinity. To fill this gap, we examine here the relationship between heme distortion and O_2 affinity. On the basis of the results of this analysis, we suggest an explanation for the strong structural distortion of the heme in Pgb and its unusual O_2 affinity.

Computational Methods

Quantum Mechanical Calculations. In the NSD framework the distortion of a porphyrin ring (D_{obs}; eq 1) is quantified from the displacements observed for C and N atoms in the structure of the macrocycle (S_{obs}) relative to a reference D_{4h} ring (S_{ref}; see eq 1). In turn, D_{obs} can be written as a linear combination of the normal mode displacements ($\hat{D}_i$; eq 2).

$$D_{obs} = S_{obs} - S_{ref} \quad (1)$$

$$D_{obs} = \sum_i d_i \hat{D}_i \quad (2)$$

where d_i is the coefficient associated with the normal mode displacement vector $\hat{D}_i$.

The most relevant (six out-of-plane and six in-plane; see Figure 1) normal modes were derived from the normal-mode analysis carried out for the geometry of a Fe(II)−porphyrin (tetracoordinated, 4c) optimized at the B3LYP/6-31G** level.[32−34] To explore the effect of the heme distortion on the O_2 binding, ad hoc distorted 4c structures (six for each mode) were built up by projecting each relevant normal mode on the porphyrin structure in both positive and negative directions until a maximum value of positional root-mean square (determined only for C and N atoms relative to the reference structure) of approximately 0.5 or 1.2 Å (for in-plane and out-of-plane distortions, respectively) which are typical values observed in the crystals. An imidazole was coordinated to the iron to simulate the environment at the active site of the proteins. The coordinated imidazole defines the proximal site in the model, leaving vacant the other side (distal) for diatomic ligand binding. Pentacoordinated (5c, distorted porphyrin and imidazole) and hexacoordinated (6c, distorted porphyrin, imidazole, and oxygen) structures were calculated as noncharged quintuplets and singlets, respectively, according to the experimental spin states.[35−37] The O_2 molecule was calculated as a triplet. Each distorted structure (X) was partially optimized, constraining all the C atom positions, but allowing geometrical relaxation of Fe, H, and N atoms of the porphyrin, the Fe-bound O_2 and the coordinated imidazole using the *modredundant* key in Gaussian'03 package. Despite each mode comprises all the C and N atoms, almost a negligible contamination was observed due to the relaxation of the N. This protocol allowed us to obtain optimized structures with an heme C-backbone distorted. 5c and 6c structures were partially optimized independently for each structure. Finally, the binding affinity was estimated from the difference between the energy of bonded and nonbonded states (eq 3).

$$\Delta E^{X}_{binding} = E^{X}_{porO_2} - E^{X}_{por} - E_{O_2} \quad (3)$$

where $E^{X}_{porO_2}$, E^{X}_{por}, and E_{O_2} denote the energy of the Fe-bound O_2, the separate porphyrin, and O_2, respectively, for a certain distorted structure X.

From a practical viewpoint, it is convenient to compare $\Delta E^{X}_{Binding}$ with the binding energy of the reference D_{4h} structure ($\Delta E^{ref}_{Binding}$), which in turn allows us to express the change in binding energy due to heme distortion ($\Delta(\Delta E)$) in terms of the energy cost due to distortion in both oxy ($\Delta E^{X}_{PorO_2}$) and deoxy (ΔE^{X}_{Por}) states of the heme (eqs 4 and 5).

$$\Delta(\Delta E) = \Delta E^{X}_{Binding} - \Delta E^{ref}_{Binding} \quad (4)$$

$$\Delta(\Delta E) = E^{X}_{PorO_2} - E^{ref}_{PorO_2} - E^{X}_{Por} + E^{ref}_{Por} = \Delta E^{X}_{PorO_2} - \Delta E^{X}_{Por} \quad (5)$$

Hybrid Quantum-Classical (QM-MM) Calculations. The initial structure for QM-MM calculations was built up starting from the crystal structure of monomeric Pgb (PDB code 2veb).[19] Molecular dynamics simulations using the AMBER force field showed that the standard parameters included for heme were not accurate enough to describe properly heme distortions. To maintain the observed distortion in the heme, we decided to alter the standard protocol used in QM-MM calculation. A minimization of the crystal structure was performed by freezing all the C's atom in heme, relaxing the system without compromising the distorted structure of the heme. Then, hybrid QM-MM geometry optimizations were performed using a conjugate gradient algorithm at the DFT level with the SIESTA code[38] using our own QM-MM implementation,[39] fixing all the C atoms in the heme. The SIESTA code showed an excellent performance for medium and large systems and also proved to be appropriate for biomolecules, and specifically for heme models.[12,40−44] Only residues located less than 10 Å apart from the heme reactive center were allowed to move freely in QM-MM runs. Calculations were performed using the generalized gradient approximation functional proposed by Perdew, Burke, and Ernzerhof.[45,46] For all atoms, basis sets of double plus polarization quality were employed as previous works showed that both QM-MM optimized structures and binding energies are properly described at this level of theory. The QM subsystem included the Fe−porphyrin ring (excluding side chains) and the relevant ligands (imidazole and O_2), while the rest of the protein and water molecules were treated classically. The scaled position link atom method[47,48] adapted to our SIESTA code was used for the interface between QM and MM regions. Further technical details about the QM-MM implementation can be found elsewhere.[49] Finally, O_2 binding energies ($\Delta E_{binding}$) were calculated as

$$\Delta E_{Binding} = E_{protO_2} - E_{prot} - E_{O_2} \quad (6)$$

where E_{protO_2}, E_{prot}, and E_{O_2} are the energy of the O_2-bound protein, the free protein, and isolated O_2.

Results

Normal Decomposition of the Penta- and Hexacoordinated Structures in the Porphyrin Ring. The NSD analysis of the fully optimized structures (nonconstrained structures) of the penta- and hexacoordinated porphyrin ring is shown in Table 1. In the pentacoordinated case (which leaves the sixth Fe coordination site immediately available for ligand binding), the principal distortions are the out-of plane negative *dom*, which indicates that the imidazole is pulling the Fe (out-of-plane), causing a doming toward the imidazole, and the in-plane negative *bre*, which indicates an expanded ring compared to the reference structure. In contrast, for the hexacoordinated structure the distortion is dominated by the *ruf* mode, while the in-plane negative *bre* distortion almost vanishes.

TABLE 1: Normal Structure Decomposition Analysis (OOP = Out-of-Plane; IP = In-Plane) of the Full-Optimized Structures of Penta- and Hexacoordinated Porphyrin Ring (in Å)

OOP	penta	hexa	IP	penta	hexa
sad	−0.030	−0.010	mst	0.000	0.036
ruf	0.000	0.234	nst	0.041	0.000
dom	−0.231	−0.043	trx	0.001	0.001
wax	0.000	−0.004	try	0.000	−0.001
way	0.001	−0.008	bre	−0.227	−0.051
pro	0.000	−0.000	rot	0.000	0.000

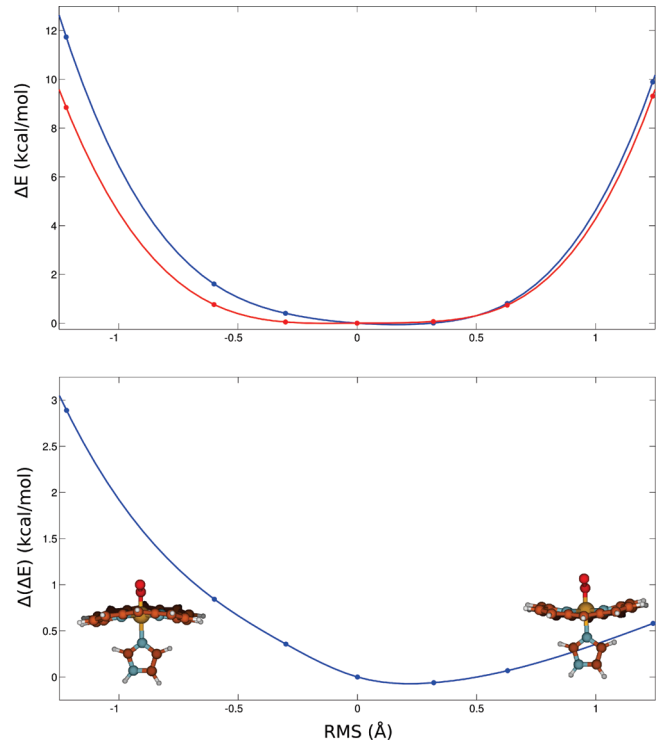

Figure 2. Top: energy cost profiles (kcal/mol) for the distortion of the heme following the *ruf* mode in oxy (blue) and deoxy (red) states. The reference value is the respective nondistorted structure (see eqs 4 and 5). Bottom: difference between the two distortion energy profiles. In the *X*-axis, the distortion value is in rms (Å).

TABLE 2: Δ(Δ*E*) (kcal/mol) Values for Selected Distortions (in Å) along Out-of-Plane Modes

	rmsd (Å)						
	−1.2	−0.6	−0.3	0.0	0.3	0.6	1.2
sad	1.9	0.5	0.1	0.0	0.1	0.5	2.4
ruf	2.9	0.8	0.4	0.0	−0.1	0.1	0.6
dom	7.0	2.6	1.0	0.0	−0.3	0.0	2.1
wax/way	3.6	0.7	0.2	0.0	0.3	1.2	3.5
pro	2.2	0.5	0.1	0.0	0.1	0.5	2.2

Effect of Out-of-Plane (OOP) Distortions on the Oxygen Affinity. The energy cost for the *ruf* distortion (see eqs 4 and 5) of the heme in both oxy and deoxy states (Figure 2) reflects an almost harmonic behavior. After the zero of both energy profiles is set at their minimum value (i.e., minimum energy structure), subtraction of both curves allows us to estimate the effect of ruffling on the O_2 binding affinity compared to that on the ideal planar ring (Δ(Δ*E*); see Figure 2). A positive *ruf* distortion leads to a slight destabilization of the binding energy (about 0.5 kcal/mol for a ruffling displacement of 1.2 Å), while negative distortions give rise to a larger destabilization (about 3 kcal/mol for a ruffling displacement of −1.2 Å).

Table 2 summarizes the corresponding Δ(Δ*E*) values for the relevant out-of-plane distortions (the corresponding energy plots are reported in Supporting Information; see Figures S1−S4). In general, all the out-of-plane distortions tend to decrease the binding affinity. Only very minor positive doming and ruffling

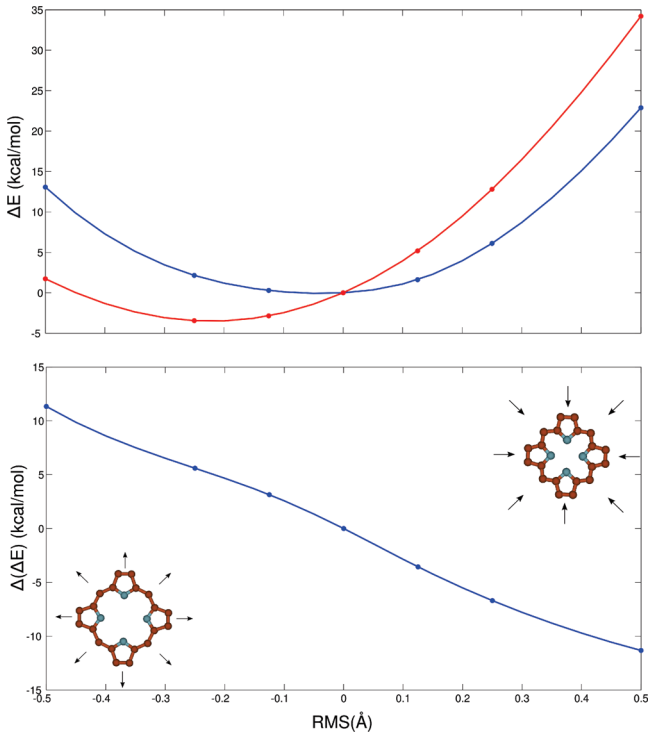

Figure 3. Top: energy cost profiles (kcal/mol) for the distortion of the heme following the *bre* mode in oxy (blue) and deoxy (red) states. The reference value is the respective nondistorted structure (see eqs 4 and 5). Bottom: difference between the two distortion energy profiles. In the *X*-axis, the distortion value is in rms (Å).

distortions lead to a very small increase in the binding affinity (by −0.3 kcal/mol at a rmsd of 0.3 Å), this effect being likely due to differences in the heme equilibrium geometry in the oxy/deoxy states. Moreover, a negative modulation of O_2 binding affinity by out-of-plane distortions is difficult to envisage, since a reduction in binding energy larger than 4 kcal/mol demands an extreme deformation of the porphyrin plane, especially for doming. On the other hand, the asymmetry observed for some of the modes can be mainly ascribed to two features: the position of the energy minimum in both penta- and hexacoordinated structures, and the curvatures of the energy profiles around the minimum energy structure. If both minima are located at nearly the same distortion value, then an almost symmetric behavior is observed.

In summary, out-of-plane distortions tend to decrease the oxygen binding energy, though the magnitude of these effects is generally small for structural distortions around the minimum energy structure, suggesting a minor contribution to modulation of the oxygen affinity in heme proteins.

Effect of the In-Plane (IP) Distortions on the Oxygen Affinity. Figure 3 shows the distortion energy determined for the *bre* mode in oxy and deoxy states. As noted above, the energy profiles exhibit an harmonic behavior. The differences in both curvatures and, principally, in the location of the minimum energy structure give rise to an interesting trend in the $\Delta(\Delta E)$ curve. First, as expected, the breathing distortion is much stiffer than out-of-plane modes, as noted in the fact that an rmsd of 0.5 Å yields $\Delta(\Delta E)$ values close to 12 kcal/mol. Second, negative displacements (i.e., an expansion of the porphyrin ring) are associated with a destabilization of the O_2 binding energy, whereas the opposite trend is found for positive displacements (i.e., a compression of the porphyrin ring).

The overall impact of the different in-plane distortions on the binding affinity can be gained from inspection of Table 3

TABLE 3: $\Delta(\Delta E)$ (kcal/mol) for Selected Positive and Negative Distortions (in Å) along In-Plane (IP) Modes

	rms						
	−0.5	−0.25	−0.125	0.0	0.125	0.25	0.5
mst	2.1	0.8	0.2	0.0	−0.3	−0.2	0.1
nst	2.0	1.1	0.3	0.0	0.3	1.1	2.0
trx/try	0.3	0.1	0.0	0.0	0.0	0.0	0.2
bre	11.3	5.6	3.1	0.0	−3.6	−6.7	−11.3
rot	2.0	0.6	0.2	0.0	0.0	0.2	1.3

(energy profiles available in the Supporting Information; see Figures S5−S8). Negative meso-stretching (*mst*) distortion reduces the binding energy, but positive displacements along this normal mode have very little impact on the O_2 affinity. In contrast, both negative and positive distortions along the N-pyrrole stretching (*nst*) decrease the O_2 binding energy. However, the most striking finding concerns breathing (*bre*), as this mode leads to an unexpected increase in the binding affinity of the heme group for O_2.

Overall, both out-of-plane and in-plane distortions tend to reduce the O_2 affinity of the porphyrin ring, even though subtle differential trends regarding the magnitude and the symmetrical behavior of such a destabilization for positive or negative displacements are found for the different normal modes. The distortion energy determined for the deoxy heme model is generally softer than that obtained for the oxy one. Accordingly, if the minima of both energy profiles are similar, an increase in the distortion is then associated with a stabilization of the pentacoordinated heme model relative to the hexacoordinated one, leading to a net reduction in the O_2 affinity of the distorted heme compared to that of the reference structure. The only exception to this general behavior involves breathing, as the substantial difference found between the minimum energy structures of penta- and hexacoordinated states makes that positive *bre* displacements increase the O_2 affinity.

Comparison of the Effect on CO Affinity. Similar calculations were carried out using CO as ligand. In Figure 4, selected modes (*bre* and *ruf*) for O_2 and CO are plotted together. As can be seen, the trends are similar for both ligands. Moreover, the fact that both ligands respond in the same way to *bre*, suggest that the effect is not an artifact. Further analysis should be done to understand the discrimination between CO and O_2. In view of these results, a reasssesment of the experimental information should be done.

Electronic Effects of Breathing Mode. The influence of the expansion−compression due to the breathing distortion on the Fe−O_2 bond can be gained from Table 4. For the nondistorted model the net charge (derived from NBO analysis) on the bound oxygen is −0.343*e*. This value is little affected upon expansion of the porphyrin ring (negative *bre* distortion). Nevertheless, while in the nondistorted heme there is an asymmetry in the charge distribution between the two oxygen atoms (O1, −0.156*e*; O2, −0.187*e*), the atomic charge is largely similar in the expanded structure (O1, −0.169*e*; O2, −0.173*e*). In contrast, porphyrin compression (positive *bre* distortion) results in increased net charge on the oxygen molecule and also in an enhanced asymmetry in the charge distribution between the two oxygens (O1: −0.161*e*; O2: −0.196*e*). With regard to the iron atom, expansion of the porphyrin ring increases the positive charge by 0.045*e*, whereas compression reduces the positive charge by 0.054*e*. Finally, the net charge of the imidazole ring remains nearly unaffected by the breathing distortion (see Table 4).

The net effect reflects an electronic density transfer from the porphyrin to the Fe-bound O_2. Thus, the overall change in the

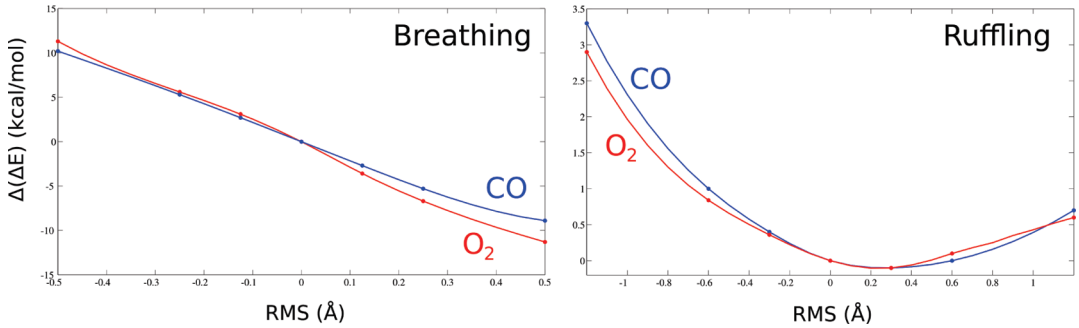

Figure 4. Δ(Δ*E*) (kcal/mol) versus distortion (Å) for CO (blue) and O_2 (red). Comparison of the *bre* (left panel) and *ruf* (right panel) modes.

TABLE 4: Comparative Analysis of the NBO Charge (in Units of e) and Bond Lengths (in Å) in the Expanded and Compressed Porphyrins[a]

bre (Å)	*d*(O−O)	*d*(Fe−O)	q_{O1}/q_{O2} (q_{O_2})	q_{Fe}	$q_{Imidazole}$
−0.5	1.268	1.737	−0.169/−0.173 (−0.342)	1.505	0.128
0.0	1.271	1.741	−0.156/−0.187 (−0.343)	1.460	0.125
0.5	1.274	1.745	−0.161/−0.196 (−0.357)	1.406	0.122

[a] q_{O1} is the charge on the oxygen closer to iron, q_{O2} is the charge on the remaining oxygen. In parentheses is the net charge on O_2.

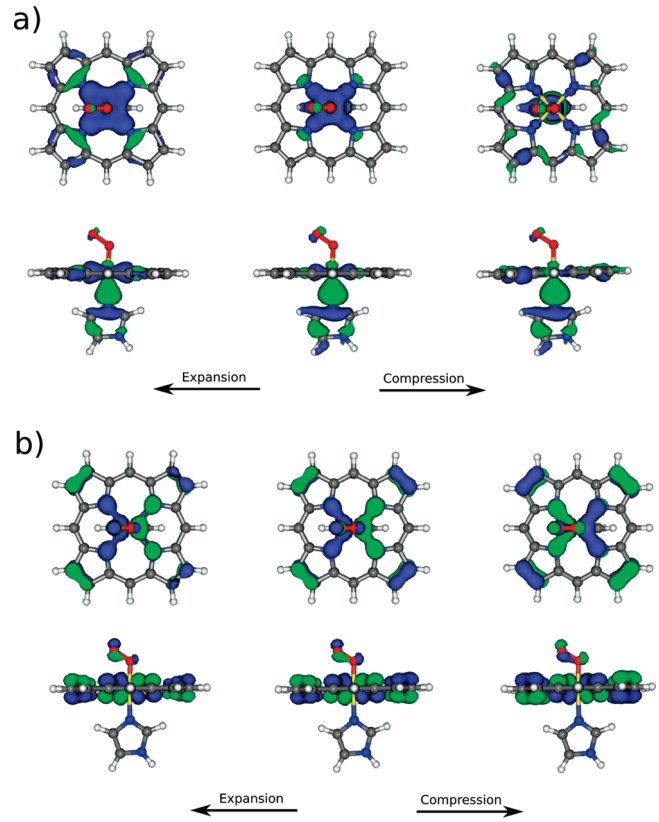

Figure 5. Side and upper views of selected NBO frontier orbitals.

Fe−O_2 charge upon expansion (+0.046*e*) or compression (−0.068*e*) of the porphyrin ring nearly matches the change in the charge of the porphyrin N atoms (−0.041*e* and +0.064*e* for expansion and compression, respectively). These changes are associated with shortening of the Fe−O1 and Fe−N_{im} bonds upon expansion of the ring, and with enlargement of those bonds upon porphyrin compression (see Table 4; see also the Supporting Information, Figure S9). As the compression proceeds, the density is "pushed" from the equatorial orbitals to the axial ones, which are then capable of interacting with both O_2 and imidazole at longer distances. Moreover, compression is accompanied by an enlargement of the O−O distance, which results from an increased population of a partially occupied antibonding orbital (see Figure S10 in the Supporting Information). It could be inconsistent that higher oxygen binding energies are not correlated with the Fe−O bond distance. However, as the binding energy arises from the comparison of two independent structures (5c and 6c) both subject to the distortion constraint, while the Fe−O distance is only observed on the 6c species, if the distortion effect is more pronounced in the 5c state, a change in the binding energy may not necessarily be correlated with Fe−O distance. Parts a and b of Figure 5a,b show selected NBO frontier orbitals located on Fe. These orbitals show clearly the effect of the *bre* mode. In (a) it can be observed that the orbitals from the pyrrolic nitrogens in the expanded structure (left) interact with the d_{z^2} of the iron. However, upon compression, this interaction is reduced, as can be observed on the enlargement of the axial component of the iron orbital. The result is that, upon compression, there exists more density on the axial component. In (b) the interaction between the pyrrolic nitrogens and the iron orbitals that participate on the Fe−O_2 bonding orbitals can be observed (see Figure S12, Supporting Information). As the compression proceeds, the orbitals become more compact. This increase in density can be transferred to the antibonding orbital of the O_2 via the iron d orbitals with proper symmetry.

Decomposition of the Pgb Oxygen Affinity. The preceding findings made us speculate that heme proteins might exploit the breathing mode to regulate the binding of ligands, since a positive/negative *bre* distortion would increase/decrease the heme−ligand affinity. In fact, the large distortion of the heme found in the 1.3 Å X-ray crystal structure of Pgb could explain the unusual low O_2 dissociation rate. At this point, it is worth noting that such a low rate cannot be justified a priori by additional interactions with the heme-bound O_2 due to the absence of distal residues able to form a hydrogen-bond with the ligand. In fact, the only distal residue that might stabilize the heme-bound O_2 is TyrB10, which has been found to provide hydrogen bonding to the heme ligand in several globins[11,12,50−52] (see Figure 6). Nevertheless, the X-ray structure of Pgb reveals that TyrB10 not only forms a hydrogen-bond interaction with the backbone of LeuE4 but is also too distant from the ligand to establish a stable hydrogen-bond interaction. This trend was confirmed from the analysis of the trajectory collected in a 500 ns molecular dynamics simulation of oxygenated Pgb. Even after reorienting TyrB10 in the starting simulation structure to favor a hydrogen-bond to the heme ligand, no significant hydrogen-bonded structure was observed (see Figure S11 in the Supporting Information).

Previous works have shown that QM/MM estimates of the O_2 binding energies are valuable to explain the O_2 dissociation rate constant in heme proteins, allowing us to detect distal,

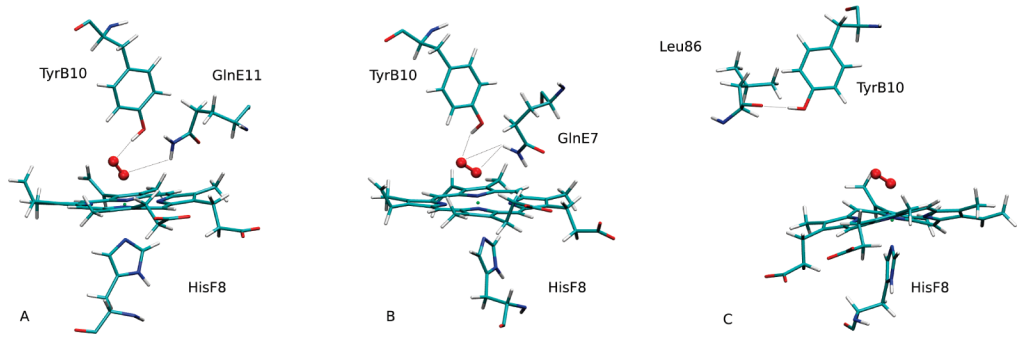

Figure 6. Active site and distal hydrogen-bond donors of *Ascaris hemoglobin* (A), *Mycobacterium tuberculosis truncated hemoglobin N* (B), and *Protoglobin* (C).

TABLE 5: Comparison between Experimental k_{off} and QM/MM Δ(Δ*E*) (kcal/mol) Relative to the Isolated Heme

protein	Δ(Δ*E*)	no. of distal HB	k_{off} (s^{-1})	ref
Pgb	−7.6	0	9.4×10^{-3} to 9.2×10^{-2}	6
Mb	−5.0	1	12	58
Mb HE7 V	−0.7	0	1600	59
trHbN	−15.2	2	0.2	58
trHbN YB10A	−7.8	1	45	60
AscHb	−12.3	2	0.4×10^{-2}	5

TABLE 6: NSD Analysis of the Heme in the Oxygenated Forms of Myoglobin (Mb, PDB code 1A6M) and Protoglobin (Pgb, PDB code 2VEB) (Distortions in Å)

OOP	Mb	Pgb	IP	Mb	Pgb
sad	−0.185	−0.390	mst	−0.017	−0.042
ruf	−0.017	+1.419	nst	−0.021	+0.006
dom	+0.206	−0.013	trx	+0.000	+0.055
wax	−0.026	−0.132	try	−0.014	+0.087
way	+0.186	+0.235	bre	−0.023	+0.202
pro	−0.071	+0.019	rot	+0.012	+0.013

proximal, and also dynamical effects.[3,12,53−57] Table 5 provides the Δ(Δ*E*) values relative to the isolated heme obtained for O_2 binding to wild type (wt) forms of Mb, AscHb, MtTrHbN, and Pgb. As expected, AscHb and MtTrHbN possess the largest increase in binding affinity (12.3 and 15.2 kcal/mol, respectively) followed by Pgb (7.6 kcal/mol) and Mb (5.0 kcal/mol), which can be explained by the presence of two (MtTrHbN, AscHb; see Figure 6) and one (Mb) hydrogen-bond between heme-bound O_2 and distal residues in the heme cavity (TyrB10 and GlnE7 in AscHb, TyrB10 and GlnE11 in MtTrHbN, and HE7 in Mb). The critical role of these hydrogen bonds on the O_2 affinity is demonstrated by the results obtained for the mutants HisE7→Val in Mb and TyrB10→Ala in MtTrHbN, which reveal a drastic decrease in Δ(Δ*E*) (see Table 5). In this context, the O_2 affinity predicted for Pgb is surprisingly large, keeping in mind the absence of stabilizing hydrogen-bonds with distal residues. In turn, it can be speculated that the origin of the intrinsic O_2 affinity found for Pgb could be related to the large distortion of the heme.

The NSD analysis of the porphyrin ring in Pgb reveals that the main out-of-plane contribution to the heme distortion is ruffling, which gives rise to a displacement of 1.42 Å, whereas the *ruf* distortion in the heme of Mb only amounts to 0.02 Å (Table 6). Regarding the in-plane distortions, the main difference between the heme moieties in Mb and Pgb affect the breathing mode, which leads to a displacement around 10-fold larger in Pgb compared to that in Mb. The presence of such a high positive *bre* distortion, and hence a high heme compression,

TABLE 7: Heme Structural Parameters for Myoglobin (1A6M), Fe(II) Porphyrin Reference, and Protoglobin (2VEB)[a]

	Mb (1A6M)	Fe(II) Por 4c (reference)	Pgb (2VEB)
d C_{meso}	6.80 ± 0.01	6.84	6.65 ± 0.04
d N_{pyrrol}	4.01 ± 0.01	3.98	3.963 ± 0.008
d C_β	8.54 ± 0.03	8.53	8.44 ± 0.04
d Fe−N	2.01 ± 0.01	1.99	1.99 ± 0.01

[a] The values are averaged (and standard deviations) in Å. See Figure 5 for the definitions.

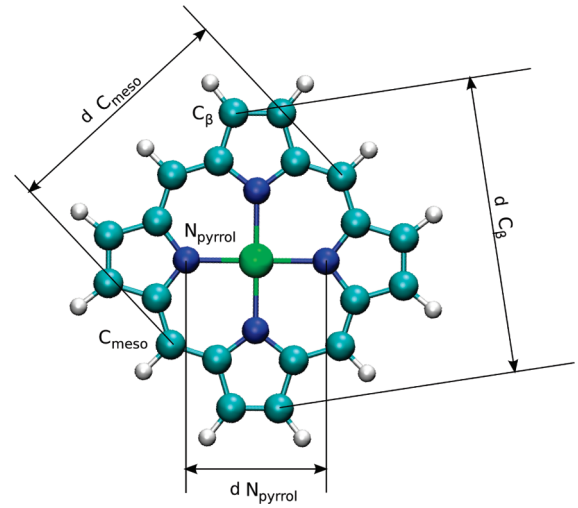

Figure 7. Definition of the structural parameters used in Table 7 to evaluate the porphyrin expansion−compression.

was never noticed before. Accordingly, both ruffling and breathing should be the main normal modes that might affect the binding properties of the heme in Pgb.

A classic view of the compression in the Pgb heme ring can be observed by measuring some structural parameters.[61] In Table 7 we present the comparison of the structural parameters exemplified in Figure 7 for the myoglobin (1A6M), the protoglobin (2VEB) and the planar porphyrin 4c reference used in the NSD analysis.

The most direct measure of the ring core is the distance between faced nitrogens (*d* N_{pyrrol}) and the Fe−N distance. While the porphyrin reference presents a value of 3.98 Å, Pgb presents a decreased value of 3.96 Å (0.02 Å from the reference) and the Mb an increased value of 4.01 Å. These values are in agreement with the *bre* distortion observed by NSD. The variation in Fe−N distance is small. For Pgb almost no modification from the reference is observed, while for Mb only a small increase is found. The distances between C_β shows a clear compression for Pgb (0.1 Å from the reference), while a

TABLE 8: Effect of the Out-of-Plane (OOP) and In-Plane (IP) Distortions Detected in Pgb on the O_2 Binding Affinity for a Heme Model System at Different Levels of Density Functional Theory (Energy in kcal/mol)

Pgb heme model	B3LYP 6-31G**	PBE 6-31G**	OLYP 6-31G**	B3LYP TZVPP (CHNO) QZVPP (Fe)	PBE (SIESTA)
OOP+IP	−3.2	−2.1	−4.3	−4.3	−2.1
Only IP	−4.7	−4.0	−5.5	−4.9	−4.1
Only OOP	1.5	1.9	1.1	0.6	2.0

negligible expansion to Mb. Finally, measuring the faced meso carbons, it can be observed that Pgb presents a high compression (0.2 Å from the reference) and Mb a minor compression. Pgb presents the three parameters in accord to a compression due to the *bre* mode, while Mb almost present the values of the reference, in agreement with the NSD.

To further explore the contribution of ruffling and breathing to the O_2 affinity, we have examined the effect of the separate distortions seen for Pgb on the binding energy in the heme model system (see Table 8). The out-of-plane distortion reduces the binding affinity, leading to a destabilization of 1.5 kcal/mol. In contrast, breathing leads to a sizable stabilization of the ligand binding energy, which clearly surpasses the destabilization due to ruffling. These changes, which agree with the trends noted above for the impact of ruffling and breathing on the binding affinity (see Figures 2 and 3 and Tables 2 and 3), indicate a net stabilization of the heme-bound O_2 compared to the ideal planar reference heme model. Notably, these trends are fully confirmed by the values determined at the PBE/6-31G**,[45,46] OLYP/6-31G**[34,62,63] and B3LYP/TZVPP/QZVPP levels[32−34] (see Table 8).

Functional Implications. Several studies have related the presence and number of hydrogen-bond interactions in the distal cavity with the O_2 binding energy and the corresponding dissociation rate.[2] Less information is available as to how much the oxygen affinity can be regulated by subtle changes in the intrinsic reactivity of the heme. The most representative examples of modulation of the dissociation rate by heme reactivity are leghemoglobin (LHb) and proximal site mutants of Mb, which affect the iron reactivity by modulating the charge density on the proximal histidine.[64] Previous QM/MM calculations from our group were able to reproduce the trend for wt and mutant Mb and LHb[12] showing that a $\Delta(\Delta E)$ of −1.6 kcal/mol results in a 3-fold increase in LHb k_{off}, while a $\Delta(\Delta E)$ of 1.4 kcal/mol yielded a 3-fold decrease in Mb dissociation rate.

Using these data as a reference, an increase of 3−5-fold of the dissociation rate can be predicted for the out-of-plane distortions generally observed in heme proteins. For the in-plane distortions, negative breathing will also result in an increase in k_{off} values. The only possibility of significantly decreasing k_{off} is the in-plane positive breathing, which may lead to a more than 5−10-fold decrease. Overall, the magnitude of $\Delta(\Delta E)$ due to moderate distortions is similar to those described previously for the proximal effects, and much smaller than those observed due to the presence of multiple hydrogen-bonds.[2]

As mentioned in the Introduction, Pgb is unusual due to both the relevant distortion of the heme and the low oxygen dissociation rate, which cannot be attributed to stabilizing hydrogen-bond interactions in the distal site. Our results point out that the observed in-plane distortion of the heme contributes to an increase in the oxygen binding affinity, which would thus agree with the available experimental data. This finding, nevertheless, raises the challenging question on how the protein moiety can induce structural distortions in the heme. Out-of-plane distortions can be promoted by the presence of bulky residues (usually leucines or phenylalanines) perpendicularly oriented to the heme plane, which may thus selectively push the pyrrole rings out of the porphyrin plane, as suggested by site-directed mutagenesis studies in the case of nitrophorins.[24] Regarding the in-plane modes, it is difficult to envisage an effective way to expand the porphyrin ring through protein interactions, as required in negative breathing. However, positive breathing can be induced by forcing the porphyrin ring to fit a tighter cavity. In this scenario, evolutionary events could subtly regulate oxygen affinity by shaping the heme cavity to favor out-of-plane distortions to decrease ligand affinity, or to compress the porphyrin ring to promote the reverse effect.

Conclusions

Our results show that heme distortions are generally expected to decrease oxygen affinity. A notable exception corresponds to positive in-plane distortions for the breathing mode, which would increase oxygen affinity. Moreover, the magnitude of the stabilization due to heme distortion can be compared to the distal and proximal effects is reported for selected heme proteins. This innovative observation suggests that the deformations of the heme moiety can be understood as an inherent modulation mechanism for ligand affinity in globins. The application to Pgb of this analysis indicates the in-plane distortion of the heme, and particularly its positive breathing mode, as a key role player in determining the high oxygen affinity observed for this protein.

Acknowledgment. This work was partially supported by the University of Buenos Aires, ANPCyT, CONICET, the Spanish Ministerio de Innovación y Ciencia (SAF2008-05595 and PCI2006-A7-0688), the Generalitat de Catalunya (2009-SGR00298), and the EU FP7 program (project NOstress).

Supporting Information Available: Energy profiles for remaining out-of-plane and in-plane mode distortions, *bre* distortion effect on Fe−O and O−O bonds, molecular dynamics details, and frontier orbitals. This material is available free of charge via the Internet at http://pubs.acs.org.

References and Notes

(1) *The Smallest Biomolecules: Diatomics and their Interactions with Heme Proteins*; Ghosh, A., Ed.; Elsevier Science: Amsterdam, 2008.
(2) Martí, M. A.; Crespo, A.; Capece, L.; Boechi, L.; Bikiel, D. E.; Scherlis, D. A.; Estrin, D. A. *J. Inorg. Biochem.* **2006**, *100* (4), 761.
(3) Scott, E. E.; Gibson, Q. H.; Olson, J. S. *J. Biol. Chem.* **2001**, *276* (7), 5177.
(4) Bikiel, D. E.; Boechi, L.; Capece, L.; Crespo, A.; De Biase, P.; Di Lella, S.; González Lebrero, M. C.; Martí, M. A.; Nadra, A.; Perissinotti, L. L.; Scherlis, D. A.; Estrin, D. A. *Phys. Chem. Chem. Phys.* **2006**, *8* (48), 5611.
(5) Goldberg, D. *Chem. Rev.* **1999**, *99*, 3371.
(6) Milani, M.; Pesce, A.; Nardini, M.; Ouellet, H.; Ouellet, Y.; Dewilde, S.; Bocedi, A.; Ascenzi, P.; Guertin, M.; Moens, L.; Friedman, J. M.; Wittenberg, J. B.; Bolognesi, M. *J. Inorg. Biochem.* **2005**, *99*, 97.
(7) Bolognesi, M.; Bordo, D.; Rizzi, M.; Tarricone, C.; Ascenzi, P. *Prog. Biophys. Mol. Biol.* **1997**, *68*, 29.
(8) Olson, J. S.; Phillips, G. N. *J. Biol. Chem.* **1996**, *271* (30), 17593.
(9) Bidon-Chanal, A.; Martí, M. A.; Estrin, D. A.; Luque, F. J. *J. Am. Chem. Soc.* **2007**, *129* (21), 6782.
(10) Boechi, L.; Martí, M. A.; Milani, M.; Bolognesi, M.; Luque, F. J.; Estrin, D. A. *Proteins* **2008**, *73* (2), 372.
(11) Crespo, A.; Martí, M. A.; Kalko, S. G.; Morreale, A.; Orozco, M.; Gelpi, J. L.; Luque, F. J.; Estrin, D. A. *J. Am. Chem. Soc.* **2005**, *127* (12), 4433.
(12) Capece, L.; Martí, M. A.; Crespo, A.; Doctorovich, F. A.; Estrin, D. A. *J. Am. Chem. Soc.* **2006**, *128* (38), 12455.
(13) Martí, M. A.; González Lebrero, M. C.; Roitberg, A. E.; Estrin, D. A. *J. Am. Chem. Soc.* **2008**, *130* (5), 1611.

(14) Collman, J. P.; Fu, L. *Acc. Chem. Res.* **1999**, *32* (6), 455.
(15) Slebodnick, C.; Ibers, J. A. *J. Biol. Inorg. Chem.* **1997**, *2* (4), 521.
(16) Jentzen, W.; Simpson, M. C.; Hobbs, J. D.; Song, X. Z.; Ema, T.; Nelson, N. Y.; Medforth, C. J.; Smith, K. M.; Veyrat, M.; Mazzanti, M.; Ramasseul, R.; Marchon, J. C.; Takeuchi, T.; Goddard, W. A., III; Shelnutt, J. A. *J. Am. Chem. Soc.* **1995**, *117*, 11085.
(17) Shelnutt, J. A.; Song, X. Z.; Ma, J. G.; Jia, S. L.; Jentzen, W.; Medforth, C. J. *Chem. Soc. Rev.* **1998**, *27*, 31.
(18) Jentzen, W.; Song, X. Z.; Shelnutt, J. A. *J. Phys. Chem. B* **1997**, *101*, 1684.
(19) Nardini, M.; Pesce, A.; Thijs, L.; Saito, J. A.; Dewilde, S.; Alam, M.; Ascenzi, P.; Coletta, M.; Ciacci, C.; Moens, L.; Bolognesi, M. *EMBO Rep.* **2008**, *9* (2), 157.
(20) Hou, S.; Freitas, T.; Larsen, R. W.; Piatibratov, M.; Sivozhelezov, V.; Yamamoto, A.; Meleshkevitch, E. A.; Zimmer, M.; Ordal, G. W.; Alam, M. *Proc. Natl. Acad. Sci. U.S.A.* **2001**, *98* (16), 9353.
(21) Vinogradov, S. N.; Hoogewijs, D.; Bailly, X.; Arredondo-Peter, R.; Gough, J.; Dewilde, S.; Moens, L.; Vanfleteren, J. R. *BMC Evol. Biol.* **2006**, *6*, 31.
(22) Freitas, T. A. K.; Hou, S.; Dioum, E. M.; Saito, J. A.; Newhouse, J.; Gonzalez, G.; Gilles-Gonzalez, M. A.; Alam, M. *Proc. Natl. Acad. Sci. U.S.A.* **2004**, *101* (17), 6675.
(23) Roberts, S. A.; Weichsel, A.; Qiu, Y.; Shelnutt, J. A.; Walker, F. A.; Montfort, W. R. *Biochemistry* **2001**, *40* (38), 11327.
(24) Shokhireva, T. K.; Berry, R. E.; Uno, E.; Balfour, C. A.; Zhang, H.; Walker, F. A. *Proc. Natl. Acad. Sci. U.S.A.* **2003**, *100* (7), 3778.
(25) Maes, E. M.; Roberts, S. A.; Weichsel, A.; Montfort, W. R. *Biochemistry* **2005**, *44* (38), 12690. 2005.
(26) Barkigia, K. M.; Chantranupong, L.; Smith, K. M.; Fajer, J. *J. Am. Chem. Soc.* **1998**, *110*, 7566.
(27) Ravikanth, M.; Chandrashekar, T. K. *Coord. Chem.* **1995**, *82*, 105.
(28) Barkigia, K. M.; Palacio, M.; Sun, Y.; Nogues, M.; Renner, M. W.; Varret, F.; Battioni, P.; Mansuy, D.; Fajer, F. *Inorg. Chem.* **2002**, *41* (22), 5647.
(29) Jarzecki, A. A.; Spiro, T. G. *J. Phys. Chem. A* **2005**, *109* (3), 421.
(30) Venkateshrao, S.; Yin, J.; Jarzecki, A. A.; Schultz, P. G.; Spiro, T. G. *J. Am. Chem. Soc.* **2004**, *126* (50), 16361.
(31) Férnandez, M. L.; Martí, M. A.; Crespo, A.; Estrin, D. A. *J. Biol. Inorg. Chem.* **2005**, *10* (6), 595.
(32) Becke, A. *J. Chem. Phys.* **1993**, *98*, 1372.
(33) Becke, A. *J. Chem. Phys.* **1993**, *98*, 5648.
(34) Lee, C.; Yang, W.; Parr, R. G. *Phys. Rev. B* **1988**, *37*, 785.
(35) Rovira, C.; Kunc, K.; Hutter, J.; Ballone, P.; Parrinello, M. *J. Phys. Chem. A* **1997**, *101*, 8914.
(36) Scheidt, W. R.; Reed, C. A. *Chem. Rev.* **1981**, *81*, 543.
(37) Momenteau, M.; Reed, C. A. *Chem. Rev.* **1994**, *94*, 659.
(38) Soler, J.; Artacho, E.; Gale, J.; García, A.; Junquera, J.; Ordejón, P.; Sánchez- Portal, D. *J. Phys. Condens. Mater.* **2002**, *14*, 2745.
(39) Crespo, A.; Scherlis, D. A.; Martí, M. A.; Ordejón, P.; Roitberg, A. E.; Estrin, D. A. *J. Phys. Chem. B* **2003**, *107*, 13728.
(40) Scherlis, D. A.; Estrin, D. A. *Int. J. Quantum Chem.* **2001**, *87*, 158.
(41) Martí, M. A.; Crespo, A.; Bari, S. E.; Doctorovich, F. A.; Estrin, D. A. *J. Phys. Chem. B* **2004**, *108*, 18073.
(42) Martí, M. A.; Capece, L.; Crespo, A.; Doctorovich, F.; Estrin, D. A. *J. Am. Chem. Soc.* **2005**, *127* (21), 7721.
(43) Martí, M. A.; Scherlis, D. A.; Doctorvich, F. A.; Ordejón, P.; Estrin, D. A. *J. Biol. Inorg. Chem.* **2003**, *8* (6), 595.
(44) Bikiel, D. E.; Bari, S. E.; Doctorovich, F. A.; Estrin, D. A. *J. Inorg. Biochem.* **2008**, *102* (1), 70.
(45) Perdew, J. P.; Burke, K.; Ernzerhof, M. *Phys. Rev. Lett.* **1996**, *778*, 3865.
(46) Perdew, J. P.; Burke, K.; Wang, Y. *Phys. Rev. B* **1994**, *54*, 16533.
(47) Eichinger, M.; Tavan, P.; Hutter, J.; Ballone, P.; Parrinello, M. *J. Chem. Phys.* **1999**, *110*, 10452.
(48) Rovira, C.; Schultze, B.; Eichinger, M.; Evanseck, J. D.; Parrinello, M. *Biophys. J.* **2001**, *81*, 435.
(49) Crespo, A.; Martí, M. A.; Estrin, D. A.; Roitberg, A. E. *J. Am. Chem. Soc.* **2005**, *127* (19), 6940.
(50) Lu, C.; Egawa, T.; Wainwrigh, L. M.; Poole, R. K.; Yeh, S. R. *J. Biol. Chem.* **2007**, *282*, 13627.
(51) Peterson, E. S.; Huang, S.; Wang, J.; Miller, L. M.; Vidugiris, G.; Kloek, A. P.; Goldberg, D. E.; Chance, M. R.; Wittenberg, J. B.; Friedman, J. M. *Biochemistry* **1997**, *36* (42), 13110.
(52) Mukai, M.; Savard, P. Y.; Ouellet, H.; Guertin, M.; Yeh, S. R. *Biochemistry* **2002**, *41* (12), 3897.
(53) Angelis, F. D.; Jarzecki, A. A.; Car, R.; Spiro, T. G. *J. Phys. Chem. B* **2005**, *109* (7), 3065.
(54) Guallar, V.; Jarzecki, A. A.; Friesner, R. A.; Spiro, T. G. *J. Am. Chem. Soc.* **2006**, *128* (16), 5427.
(55) Spiro, T. G.; Jarzecki, A. A. *Curr. Opin. Chem. Biol.* **2001**, *5* (6), 715.
(56) Martí, M. A.; Bikiel, D. E.; Crespo, A.; Nardini, M.; Bolognesi, M.; Estrin, D. A. *Proteins* **2005**, *62* (3), 641.
(57) Martí, M. A.; Capece, L.; Bikiel, D. E.; Falcone, B.; Estrin, D. A. *Proteins* **2007**, *68* (2), 480.
(58) Milani, M.; Pesce, A.; Nardini, M.; Ouellet, H.; Ouellet, Y.; Dewilde, S.; Bocedi, A.; Ascenzi, P.; Guertin, M.; Moens, L.; Friedman, J. M.; Wittenberg, J. B.; Bolognesi, M. *J. Inorg. Biochem.* **2005**, *99*, 97.
(59) Kundu, S.; Snyder, B.; Das, K.; Chowdhury, P.; Park, J.; Petrich, J. W.; Hargrove, M. S. *Proteins* **2002**, *46*, 268.
(60) Couture, M.; Yeh, S.; Wittenberg, B. A.; Wittenberg, J. B.; Ouellet, Y.; Rousseau, D. L.; Guertin, M. *Proc. Natl. Acad. Sci. U.S.A.* **1999**, *96*, 11223.
(61) Kozlowski, P. M.; Bingham, J. R.; Jarzecki, A. A. *J. Phys. Chem. A* **2008**, *112*, 12781.
(62) Handy, N. C.; Cohen, A. J. *Mol. Phys.* **2001**, *99*, 403.
(63) Hoe, W.-M.; Cohen, A. J.; Handy, N. C. *Chem. Phys. Lett.* **2001**, *341*, 319.
(64) Kundu, S.; Trent, J. T., III; Hargrove, M. S. *Trends Plant Sci.* **2003**, *8*, 387.

JP102135P